Study of Porous Silicon Nanostructures as Hydrogen Reservoirs

ARTICLE *in* THE JOURNAL OF PHYSICAL CHEMISTRY B · OCTOBER 2005

Impact Factor: 3.3 · DOI: 10.1021/jp053007h · Source: PubMed

9 AUTHORS, INCLUDING:

S. A. Alekseev
National Taras Shevchenko University of Kyiv
63 PUBLICATIONS **312** CITATIONS
SEE PROFILE

Vladimir N. Zaitsev
Pontifícia Universidade Católica do Rio de Ja…
139 PUBLICATIONS **747** CITATIONS
SEE PROFILE

Francesco Geobaldo
Politecnico di Torino
141 PUBLICATIONS **3,650** CITATIONS
SEE PROFILE

Edoardo Garrone
Politecnico di Torino
286 PUBLICATIONS **7,316** CITATIONS
SEE PROFILE

Study of Porous Silicon Nanostructures as Hydrogen Reservoirs

Vladimir Lysenko,* Fabrice Bidault, Sergei Alekseev,† Vladimir Zaitsev,† and Daniel Barbier

Materials Physics Laboratory, LPM, CNRS UMR-5511, INSA de Lyon, 7 avenue Jean Capelle, Bat. Blaise Pascal, 69621 Villeurbanne Cedex, France

Christophe Turpin

Electrical Engineering and Industrial Electronics Laboratory, LEEI, CNRS UMR-5828, INP de Toulouse, 2 rue Camichel, BP-7122, 31071 Toulouse Cedex 7, France

Francesco Geobaldo, Paola Rivolo, and Edoardo Garrone

Department of Material Science and Chemical Engineering, Politecnico di Torino, Corso Duca degli Abruzzi 24, 10129 Torino, Italy

Received: June 6, 2005; In Final Form: August 18, 2005

The amount of hydrogen present in porous silicon (PS) nanostructures is analyzed in detail. Concentration of atomic hydrogen chemically bound to the specific surface of PS is quantitatively evaluated by means of attenuated total reflection infrared (ATR-IR) spectroscopy and temperature-programmed desorption (TPD) spectroscopy. The concentration values are correlated to the PS nanoscale morphology. In particular, the influence of porosity, silicon nanocrystallite dimension, and shape on hydrogen concentration values is described. Hydrogen concentrations in fresh, aged, as well as in chemically and thermally treated PS layers are measured. Maximal hydrogen concentration of 66 mmol/g is detected in nanoporous layers with high (>95%) porosity consisting of nanocrystallites with dimensions of about 2 nm. Mass energy density that can be potentially obtained from this amount of hydrogen through a low-temperature fuel cell is estimated to be about 2176 W-h/kg and is found to be comparable with other substances containing hydrogen, such as hydride materials and methanol, which are usually used as hydrogen reservoirs.

I. Introduction

During the past few years, particular efforts have been undertaken to assemble silicon-based microfuel cells to supply portable devices.[1−3] Finding simple ways for hydrogen storage in such types of microsystems that can be directly compatible with silicon-based microtechnologies is one of the key issues. Different hydrogen containing materials, such as hydrides and carbon nanostructures, are already studied and proposed for hydrogen storage application.[4] However, these materials are not really compatible with the silicon microtechnologies. It would, therefore, be ideal to construct silicon-based hydrogen tanks. In this paper, hydrogen content in porous silicon (PS) nanostructures is quantitatively analyzed from a structural and energetic point of view while keeping in mind the possible application of the nanostructures in the future as hydrogen reservoirs.

The huge internal specific surface (up to 1000 m^2/cm^3)[5] of PS nanostructures is covered by SiH_x bonds.[6] Hydrogen influences significantly all physical properties of the Si nanocrystallites constituting PS nanostructures. For example, hydrogen coverage is found to be responsible for the expansion of nanocrystallites,[7] modifying consequently their electronic properties.[8] PS nanostructures were recently observed to be strongly explosive,[9,10] and one of the key reasons for this phenomenon is the significant amount of hydrogen chemically bound to the PS surface. Emission of molecular hydrogen (H_2) produced from the heat-induced decomposition of SiH_x groups homogeneously covering the PS nanostructures[11,12] allows putting forward such a material for its application as a hydrogen reservoir. Rivolo et al.[11] have recently performed a measurement of the total amount of molecular hydrogen thermally desorbed from a 120 μm thick 60% mesoporous free-standing layer and a value of 2 mmol/g was found. Other authors announced only rough estimations of the hydrogen amount adsorbed on the PS-specific surface (see, for example, refs 6, 9). The results of Rivolo et al.[11] were confirmed later[13] from detailed analysis of atomic hydrogen concentration in the meso-PS nanostructures as a function of their nanoscale morphology. In particular, maximum values of atomic hydrogen concentration were found to be 15 mmol/g at 90% porosity.[13] To increase hydrogen concentration values, one should increase the PS-specific surface by decreasing the dimensions of the silicon nanocrystallites constituting the porous layer. It can be achieved by using p-type silicon wafers with low doping levels ($10^{16}/cm^3$) that allow the formation of nano-PS layers with smaller nanocrystallites (<7 nm), contrary to the meso-PS samples consisting of larger nanocrystallites (7−20 nm) and formed on highly doped ($10^{19}/cm^3$) silicon wafers.

In this paper, we analyze the hydrogen content of PS nanostructures for their application as emergency hydrogen reservoirs for microfuel cells. The amount of hydrogen chemically bound to the specific surface of the nano-PS structures is

* Corresponding author. E-mail: vladimir.lysenko@insa-lyon.fr.

† Permanent professional address: Analytical Chemistry Department, Chemical Faculty, National Tarasse Shevchenko University, 64 Vladimirskaya Str., 01033 Kiev, Ukraine.

10.1021/jp053007h CCC: $30.25
Published on Web 09/30/2005

studied as a function of their nanoscale morphologies. The obtained results are compared with the case of meso-PS nanoscale morphologies reported earlier.[13] In particular, the influence of porosity, nanocrystallite dimension, and shape on the hydrogen concentration is analyzed. Reproducibility and stability of the hydrogen content in the PS nanostructures as well as chemically and thermally stimulated hydrogen desorption are reported. Conversion of the experimentally detected hydrogen concentrations into electrical energy through fuel cells is theoretically estimated.

II. Experimental Section

II.1. Porous Silicon Formation. The PS samples used in this study were produced according to a standard procedure[14] based on electrochemical etching of monocrystalline (100)-oriented boron-doped Si wafers (1−10 Ω cm and 0.01 Ω cm for nano- and meso-PS structures, respectively) at current densities of 2−340 mA/cm^2. The etching solutions of 9:1, 3:1, and 1:1 mixtures (by volume) of concentrated aqueous hydrofluoric acid (48%) and ethanol were used for nano-PS formation and an HF/ethanol solution of 1:1 volume mixture for meso-PS formation.

II.2. Structural Characterization of Porous Silicon. Depending on the current density and on the composition of the etching solution, the porosity of the layers was estimated from the PS refractive index measurements performed by means of a Perkin-Elmer GSX-2 Fourier transform infrared (FTIR) spectrometer used in reflective backscattering geometry and from the correlation of the index values to porosity by using Bruggeman's effective media model.[15] The PS refractive indexes were deduced from the spectral position of the interferential fringes detected for the optically thin PS samples using the following relationship:

$$n_{PS} = \frac{1}{2d}\left(\frac{1}{\lambda_k} - \frac{1}{\lambda_{k+1}}\right)^{-1} \quad (1)$$

where d denotes the thickness of the porous layer and λ_k is the wavelength of the kth fringe. The thickness of all porous films determined from optical microscopy measurements was about 10 μm. The dimension of Si nanocrystallites constituting the porous layers was estimated by Raman microspectroscopy by using a method described in details elsewhere.[16]

II.3. Attenuated Total Reflection (ATR) FTIR Spectroscopy. Hydrogen concentration in the fresh as-prepared PS samples was evaluated from the infrared absorption spectra of the stretching vibrations of Si−H$_x$ bonds. The spectra were collected by using the FTIR spectrometer in the attenuated total reflection (ATR) measurement mode. These kinds of measurements were performed on the mechanically stable 10-μm-thick PS layers. The PS samples were placed on a germanium single crystal with refractive index $n_{Ge} = 4$ used for infrared wave guiding and ensuring an incident beam angle $\theta = 45°$. To obtain the adsorption spectra, the dependence of the penetration depth of the evanescent waves into the PS sample, d_e, on their wavelength, λ, and on the PS refractive index, n_{PS}, was considered according to the following relation:[17]

$$d_e = \frac{\lambda}{2\pi n_{Ge}\sqrt{\left[\sin^2\theta - \left(\frac{n_{PS}}{n_{Ge}}\right)^2\right]}} \quad (2)$$

Hydrogen concentration N_H (mmol g^{-1}) was estimated from the absorption spectra by using the following relation used earlier for the estimation of hydrogen content in amorphous Si layers:[13]

$$N_H = \frac{1}{\Gamma_S \rho_{Si}(1-P)}\int_{h\upsilon}\frac{\alpha}{h\upsilon}\,d(h\upsilon) = \frac{I_S}{\Gamma_S \rho_{Si}(1-P)} \quad (3)$$

where I_S (cm^{-1}) is the integrated adsorption of the stretching band, ρ_{Si} is the monocrystalline Si density (2.33 g cm^{-3}), P is the porosity of the PS layer, α (cm^{-1}) is the absorption coefficient, $h\upsilon$ is the photon energy, and Γ_S (cm^2 mmol^{-1}) is the stretching oscillator strength of the Si−H bonds, which was determined from the following relationship[13] as it was proposed for amorphous silicon:

$$\Gamma_S = 37.6 \times \frac{I_S}{I_W} \quad (4)$$

where I_S and I_W are experimentally measured integrated adsorption of the stretching and wagging (near 640 cm^{-1}) bands, respectively.

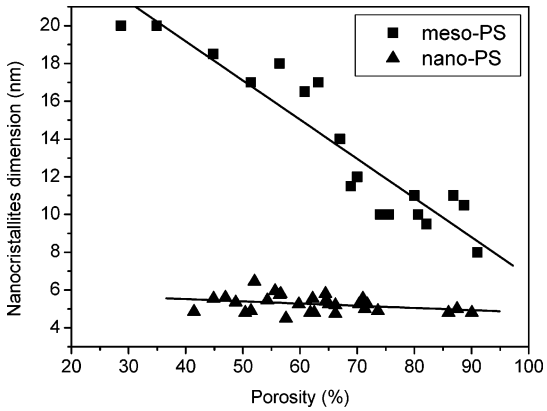

Figure 1. Dimensions of Si nanocrystallites in meso- (■) and in nano-PS (▲) layers vs porosity. Straight solid lines represent linear fits of the experimental data.

II.4. Temperature-Programmed Desorption (TPD). A TPD setup allows studying of the temperature-resolved desorption of hydrogen from the PS samples. The TPD studies have been performed in a quartz reactor, in the range of 40−1000 °C by means of a Thermoquest TPD/R/O 1100 analyzer. The signal recorded by a thermal conductivity detector during programmed heating of a PS sample is the difference in thermal conductivity between the inert gas (argon) flowing in the reference arm and the gas in the measurement arm, comprising gaseous species released from the sample. A quadruple mass analyzer (Baltzer Quadstar 422) coupled to the TPD apparatus allows the identification of desorbed species. To obtain quantitative measurements on the molecular hydrogen desorbed from the sample specific surface, calibration has been performed by injecting known amounts of hydrogen into the argon flow and evaluating the area of the detected TPD signal. The PS powder obtained from the mechanically instable PS layers has been used for these experiments.

III. Hydrogen in Porous Silicon Nanostructures

III.1. Nanoscale Morphology of the Meso- and Nano-PS Layers. Figure 1 shows the evolution of the dimension, d, of the Si nanocrystallites constituting the PS layers. The nanocrystallites forming the meso-PS structures are larger than those from the nano-PS layers in all porosity ranges. In the case of the meso-PS, the nanocrystallite dimension decreases progres-

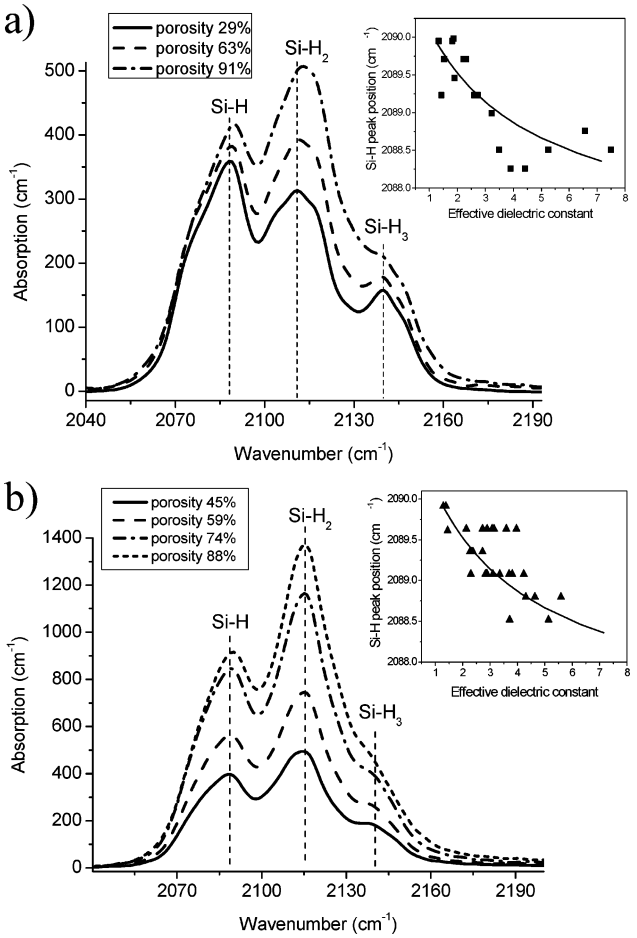

Figure 2. Infrared absorption spectra of as-prepared hydrogenated meso- (a) and nano-PS (b) layers for different porosity values. Inserts show a shift of the Si−H peaks along with effective dielectric constant of the PS nanostructures (see discussion in text).

sively from 20 nm down to 8 nm as porosity increases in the range of 30−90%. As for the nano-PS layers, the dimensions of the nanocrystallites constituting these layers are found to be quasiconstant around 5 nm (only an extremely slight decrease can be observed) in all porosity ranges. In this case, the increase in porosity is ensured by a decrease in the number of nanocrystallites.

Assuming a smooth spherical geometry of the nanocrystallites, specific surface area of the PS nanostructures, S (m^2/g), can be roughly estimated from the dimension values using the following relationship: $S = 6/d_{PS}\rho_{Si}$, where d_{PS} is the nanocrystallite dimension and ρ_{Si} is the monocrystalline Si density ($2.33\ g/cm^3$). From this relationship, the specific surface values corresponding to 60% porosity are found to be 150 and 515 m^2/g for meso- and nano-PS nanostructures, respectively, in good accordance with the experimental data reported in the literature.[18]

III.2. SiH_x Bond Analysis from FTIR Spectral Features. Typical well-known $Si-H_x$ (with $x = 1, 2, 3$) stretching vibration spectra of meso- and nano-PS nanostructures are shown in Figure 2. Three well-defined large bands centered at 2088, 2110, and 2137 cm^{-1} mainly corresponding respectively to Si−H, $Si-H_2$ and $Si-H_3$ stretching bonds can be clearly seen. Additionally, a fine structure of the absorption bands consisting of about seven overlapping peaks can be distinguished (especially for a low-porosity meso-PS sample), which is probably due to the specific orientations of $Si-H_x$ bonds in space induced by morphological anisotropy of Si nanocrystallites constituting the porous nanostructures, as it was recently demonstrated by Timoshenko et al.[19] In particular, oscillation modes corresponding to Si monohydride dimmers can also be present in the range of 2075−2103 cm^{-1}.[19]

A slight spectral shift of the Si−H and $Si-H_2$ bands toward high energies as porosity increases is observed in Figure 2 for both meso- and nano-PS nanostructures. This can be explained by the influence of the porosity-dependent effective dielectric constant on the binding energy of SiH_x bonds. Indeed, the decrease of the dielectric constant with porosity leads to the enhancement of the SiH_x binding energy and, consequently, to a shift of their vibration frequencies toward a higher energy edge, as shown in Figure 2. The experimental points corresponding to the SiH peak positions (see inserts in Figure 2a and b) can well be fitted (solid curve) by the following expression proposed by Wieder et al.:[20]

$$\omega_{SiH} = \sqrt{\omega_0^2 - A\frac{\epsilon_{PS} - 1}{\epsilon_{PS} + 3}} \qquad (5)$$

where ω_{SiH} is the energy of the SiH peak, ω_0 and A are the fitting parameters (same for the meso- and nano-PS) equal (in our case) to 2090.1 cm^{-1} and to 1.2×10^4 cm^{-2}, respectively, and $\epsilon_{PS} = n_{PS}^2$ is the porosity-dependent effective dielectric constant of the PS samples.

Another porosity-induced effect can also be observed from the absorption spectra of the meso-PS layers (Figure 2a). Indeed, the peak corresponding to the Si−H band is more intense than that of the $Si-H_2$ band for low porosity values (<63%). Thus, hydrogen is bound to Si atoms by forming mainly monohydride groups. For high porosity values (>63%), hydrogen is mainly stored in silicon dihydride complexes, while for intermediate porosity (≈63%), the peak absorption intensities of the mono- and dihydride bonds are the same. To our minds, such a porosity-dependent remarkable progressive evolution of the $Si-H_2$ peak in comparison with the negligible changes of the Si−H peak can be explained by the increase of fractal-like roughness of the Si nanocrystallite surfaces, favoring additional appearance of surface Si atoms allowing the formation of the $Si-H_2$ and Si−H dimer complexes.[13] Being relatively smooth (the roughness level is negligible in comparison with the nanocrystallite dimensions) at low porosities (<63%), the large nanocrystallites contains mainly surface Si atoms with only one unsaturated bond, which is, therefore, able to bind only one hydrogen atom. Porosity increase accompanied by the nanocrystallite dimension reduction (see Figure 1) leads to a relative increase of the nanocrystallite fractal-like surface roughness and, consequently, to the enhancement of the number of SiH_2 bonds.

As for the nano-PS samples (Figure 2b), the small dimensions (≈5 nm) of the PS nanocrystallites are comparable or even smaller than the fractal-like surface roughness that leads to a high number of silicon dihydride bonds with respect to the monohydride ones independently of the porosity value, as reflected by the corresponding spectra (Figure 2b). The fractal nature of the nanocrystallite surface is further confirmed below by independent hydrogen concentration measurements.

III.3. Hydrogen Concentration Measurements. Figure 3 shows the variation of the atomic concentration of hydrogen bound to Si atoms at the PS-specific surface as a function of the porosity of the layer. In general, the concentration variation with porosity reflects structural evolution of the PS-specific surface to which hydrogen is bound. Hydrogen concentration values in nano-PS are higher than in meso-PS layers because of the much more important specific surface to which hydrogen

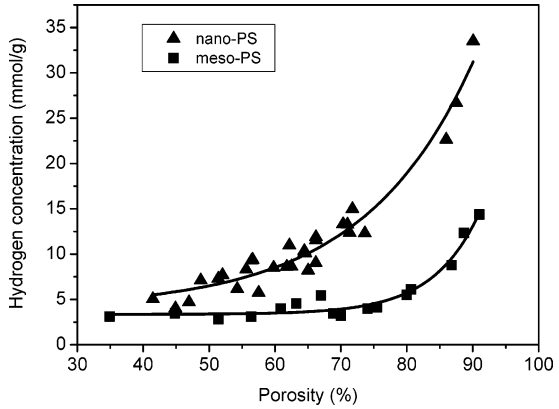

Figure 3. Hydrogen concentration variation along with porosity in meso- (■) and nano-PS (▲) layers. Solid lines added as eye guides represent exponential fit of the experimental data.

atoms may be bound. Indeed, as it was already observed from nitrogen adsorption experiments,[18] the specific surface of meso-PS is measured to be about 200 m^2/cm^3, while the nano-PS surface is found to be about 600 m^2/cm^3. Such an important difference of the specific surface values for the meso- and nano-PS morphologies are explained by the difference of the nanocrystallite dimension constituting these two PS morphological types, as can be seen in Figure 1. Indeed, for a given porosity value, the smaller the nanocrystallite dimension is, the higher the corresponding specific surface is.

Concerning the meso-PS samples (Figure 3) in the 30−70% porosity range, the hydrogen concentration is very low and relatively constant (2.5−5 mmol/g) because the samples are characterized by large (Figure 1) and smooth nanocrystallites. For example, the concentration of atomic hydrogen at the surface of the meso-PS sample of 60% porosity is 3.8 mmol/g that corresponds well to the value of the molecular hydrogen extracted by Rivolo et al.[11] from thermal desorption measurements (≈2 mmol/g). Despite the nanocrystallite decrease from 20 to 12 nm, the corresponding specific surface values remain still too small (125−200 m^2/g) in the meso-PS samples with porosities <70%. The corresponding quantity of hydrogen bound at this surface is also too small to be measured with good precision. Therefore, only a slight variation of the hydrogen concentration around a constant level is found in this porosity range. Despite the almost unchangeable nanocrystallite dimensions around 10 nm, a monotonic exponential increase of the concentration (up to 13 mmol/g) in the range of high porosities (>70%) reflects an important enhancement of the PS-specific surface induced by the extremely developed fractal-like surface roughness of the Si nanocrystallites constituting the porous layers, as it was already concluded from the FTIR spectrum feature analysis described in the previous chapter.

The fractal nature of the PS-specific surface roughness is completely confirmed by hydrogen concentration analysis in the nano-PS samples. Indeed, as it can be seen in Figure 3, the concentration of hydrogen increases exponentially along with porosity. An excellent exponential fit of the experimental data is represented in Figure 3 by a solid line. Quasiconstant values of the Si nanocrystallite dimensions along all porosity ranges (see Figure 1) means that the porosity increase is ensured only by the decrease of the number of nanocrystallites, and consequently, the observed increase of the total specific surface with porosity is possible only if an important enhancement of the fractal-like surface roughness at the nanometer scale is considered for each nanocrystallite. Fractal parameters (dimension and lacunarity) of the nanocrystallites constituting the nano-PS

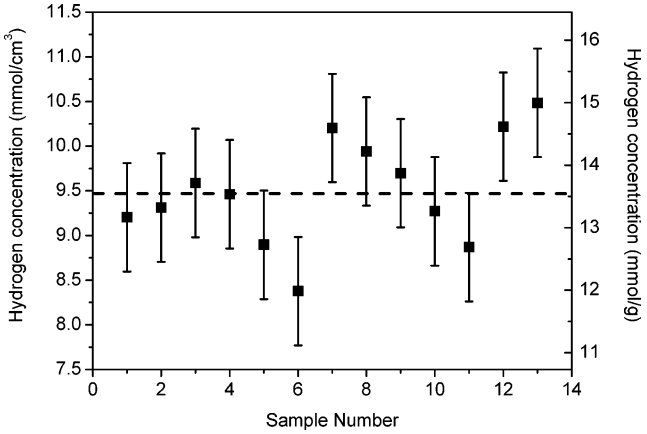

Figure 4. Reproducibility of hydrogen content in nano-PS. Thirteen nano-PS samples were fabricated under the same anodization conditions: anodization current density, 220 mA/cm^2; HF/ethanol ratio, 9:1.

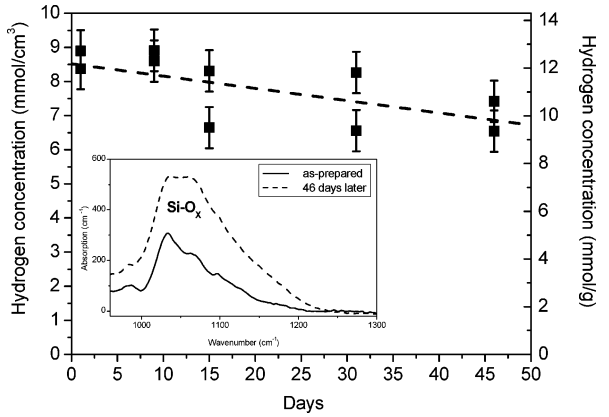

Figure 5. Natural loss of hydrogen during the aging of the PS sample at atmospheric pressure and ambient temperature. The insert shows FTIR adsorption spectra of Si−O_X band, reflecting an increase of the silicon oxide amount accompanying the porous sample aging.

structures are deduced from a model described in one of our earlier papers.[21] The porosity-dependent fractal shape of the PS-specific surface ensures a maximum value for the hydrogen concentration achieved at the highest porosities (90% for both meso- and nano-PS structures).

III.4. Reproducibility and Stability of the Hydrogen Content in PS Nanostructures. Figure 4 shows reproducibility of the hydrogen content in the nano-PS samples. Thirteen such samples were formed at the same anodization conditions (anodization current density: 220 mA/cm^2, HF/ethanol ratio 9:1). The maximal deviation from the mean value (9.5 mmol/g) is found to be about ±10%. Figure 5 represents natural loss of hydrogen by nano-PS during its storage at atmospheric pressure and ambient temperature. After 50 days of storage, the PS sample has lost about 18% of the initial quantity of hydrogen. The loss of hydrogen is accompanied by an increase of silicon oxide amount due to spontaneous oxidation of PS nanocrystallites in ambient air, as can be concluded from the growth of the IR absorption band corresponding to the Si−O vibrations (see insert in Figure 5).

III.5. Thermally Stimulated Desorption of Hydrogen. Further dimension decrease (down to 2−3 nm) of the PS nanocrystallites showing high photoluminescent efficiency should additionally increase PS-specific surface and, consequently, the amount of the chemically bound hydrogen. Such samples were fabricated at anodization current densities of 70 mA/cm^2 in a 1:1 mixture (by volume) of concentrated aqueous

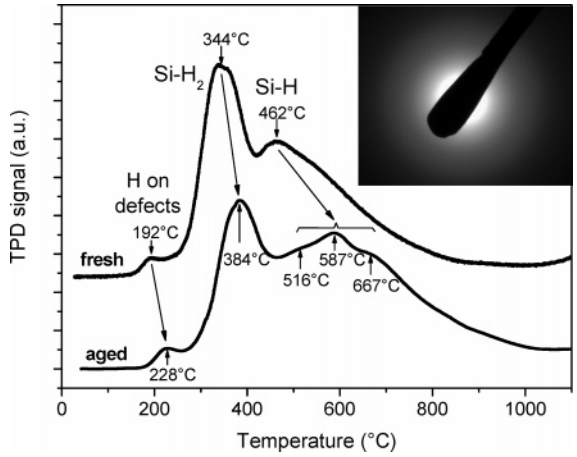

Figure 6. Effusion curves for H_2 desorption from fresh and aged nano-PS samples. Electron diffraction image given in insert reflects amorphous structure of the PS samples.

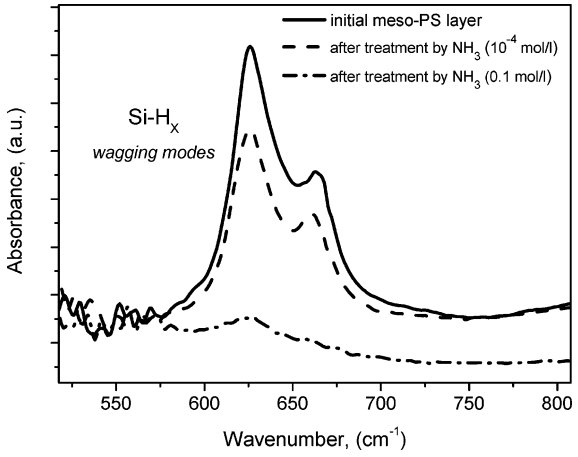

Figure 7. Chemically stimulated desorption of hydrogen from meso-PS layers. IR absorption spectra of Si−H_x wagging band corresponding to the hydrogenated meso-PS layers treated by NH_3 solutions.

hydrofluoric acid (48%) and ethanol. Small nanocrystallite dimension (2−3 nm) and high porosity (>95%) result in poor mechanical stability of the formed samples. Indeed, partial destruction of the PS samples occurs during their drying, which leads to the transformation of the nano-PS layer into a powder state. Because the use of FTIR-ATR setup for measuring hydrogen quantity in such samples becomes too problematic, the amount of hydrogen present in the samples was measured by the TPD technique described above.

Figure 6 reports TPD signals obtained on the fresh and aged (50 days storage) PS samples. Comparison between TPD curves and mass spectrum of the desorbed species shows that the desorbed phase is almost completely constituted by H_2.[11] A negligible contribution from desorbed silanes is found to be at least 2 orders of magnitude lower than that observed for hydrogen.[11] Three main regions corresponding to the hydrogen desorption from the fresh PS sample are present in Figure 6: (i) a weak signal at 190 °C, (ii) a more intense one centered at 350 °C, and (iii) another one situated around 460 °C. The two last intensive peaks related to the hydrogen desorption from Si−H_2 and Si−H bonds were already observed by Martin et al.[12] on PS formed on *n*-type Si wafers. The first low-temperature peak is assumed to correspond to hydrogen desorption from numerous structural defects present in the high nanoporous samples. Indeed, as indicated by the electron diffraction image (see insert in Figure 6), the PS samples used for the thermally stimulated desorption study have amorphous structure, and therefore, atomic and/or even molecular hydrogen can be easily trapped in such completely disordered PS nanostructures.[22] TPD signal of the PS sample after about 50 days of storage mainly preserves its general shape and is shifted by about 40 °C toward the higher temperatures in comparison with the signal from the fresh samples. This shift corresponds to the storage-induced slight oxidation of the PS samples (see Figure 5), resulting in a slight increase of binding energies of Si−H_x bonds in which the Si atoms are back-bonded to one or more oxygen atoms, as was earlier deduced from IR spectroscopy.[23] In addition, the Si−H region becomes much broader in the aged samples, with three clear shoulders indicated in Figure 6. This last observation is in good agreement with the TPD observation performed earlier on meso-PS samples.[11]

The integration of the TPD signal corresponding to the fresh PS sample yielded a maximal value of the total amount of desorbed molecular hydrogen (H_2) being around 33 mmol/g. It corresponds to 66 mmol/g of atomic hydrogen chemically bound at the PS-specific surface. Taking into account that 1 g of Si contains 36 mmol of Si atoms, one can roughly conclude that each Si atom in the PS sample is bound to 2 hydrogen atoms. From the fractal model point of view, it means that the fractal dimension of the nanoparticles constituting the PS samples tends toward 2. This conclusion is in excellent agreement with our fractal model elaborated for the hydrogenated PS nanostructures.[21] In other words, the small (1−3 nm) nanocrystallites constituting the nano-PS layer can be represented as a binary solid constituted by Si and H atoms. Such enormous hydrogen content can be partially responsible for structural disorder detected in the PS samples (see insert in Figure 6).

III.6. Chemically Stimulated Desorption of Hydrogen. It is well-known that Si−H bonds in the organic compounds react quite easily with water in the presence of bases.[24] Evolution of H_2 and formation of Si−O bonds are the results of the following reaction:

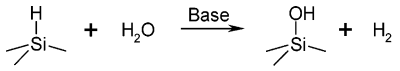

(A)

Such kinds of reactions can be used for hydrogen desorption from the surface of meso- and nano-PS layers. In our work, the PS samples were treated with water solutions of a weak base (NH_3) during 20 min. The concentration of the NH_3 solution was in the range of 10^{-4}−0.1 mol/L. The reaction A accompanied by H_2 gas bubbling was clearly observed for all of the studied samples and for all of the used concentrations of the NH_3 solutions. Evolution of the hydrogen coverage provoked by the treatment of the meso-PS samples of 70% porosity with NH_3 solutions was monitored by FTIR-ATR spectroscopy. As it can be seen in Figure 7, the intensity of the Si−H_x wagging band near 640 cm^{-1} decreases to 25% after the sample treatment by the solution with the lowest NH_3 concentration, i.e., 10^{-4} mol/L. It should be mentioned that the quantity of NH_3 molecules in such a solution is at least 50 times lower than the quantity of Si−H_x groups in the treated sample. Therefore, the ammonia acts rather as a catalyst than as a reagent in this reaction. In contrast, a treatment with 0.1 mol/L NH_3 solution results in complete desorption of hydrogen from the PS surface, which is illustrated in Figure 7 by the disappearance of the Si−H_x wagging band. Treatment of the nano-PS samples of 80% porosity with 10^{-4} mol/L NH_3 solutions results in a 75% decrease of Si−H wagging band. The increase of the treatment efficiency of the nano-PS in comparison with the meso-PS

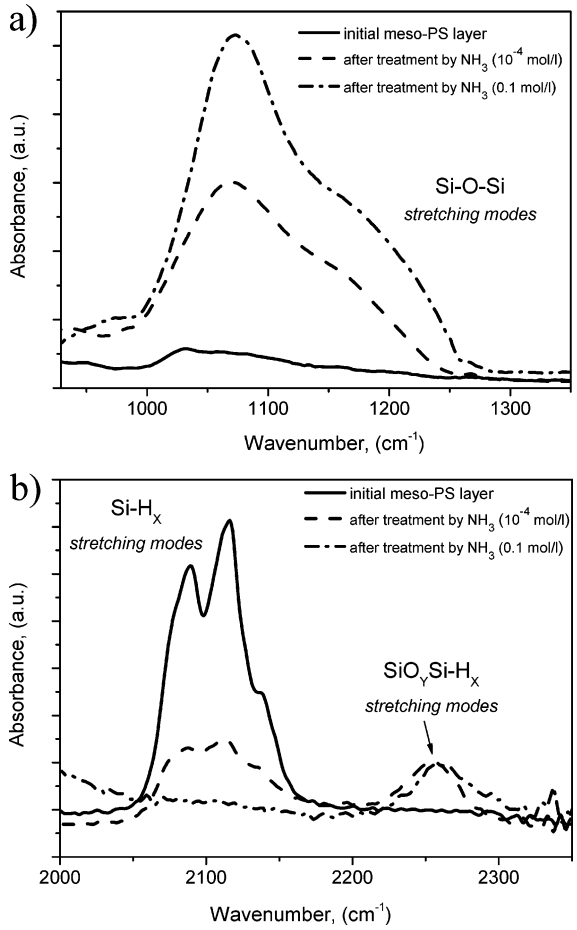

Figure 8. IR absorption spectra of: (a) Si−O−Si stretching band and (b) SiO_ySi-H_x band appeared in the PS samples after hydrogen desorption stimulated by NH_3 solutions.

samples is due to the much higher values of the specific surface in the nano-PS structures. In particular, treatment of the nano-PS layers with higher NH_3 concentrations (up to 10^{-3} and 10^{-2} mol/L) results in a complete removal of the layers from the underlying Si substrate. It can be explained by the breaking of the Si−Si bonds in the mechanically unstable nanocrystallites during their reconstruction provoked by the hydrogen desorption.

It should also be mentioned that reaction A is not the single one taking place during the treatment of the PS samples with bases. Indeed, adsorption bands situated near 2260 cm^{-1} (stretching of Si−H bonds in SiO_ySiH_x complexes) and near 1100 cm^{-1} (stretching of Si−O−Si fragments) present in the IR spectra of the PS samples treated with NH_3 solutions (see Figure 8) indicate the interaction of water with numerous highly reactive Si dangling bonds (see reaction scheme B) appearing at the nanocrystallite surface after the hydrogen release induced by the initial reaction A:

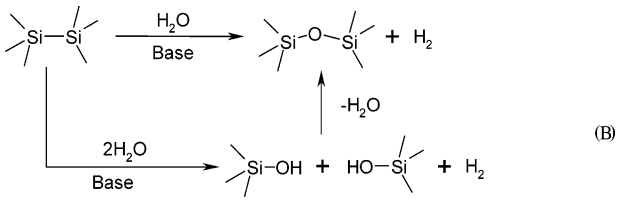

(B)

In particular, reaction of the nano-PS samples constituted by the small Si nanoparticles (5 nm in diameter) with 0.1 mol/L NH_3 results in a complete conversion of the PS nanostructure into hydrated dioxide ($SiO_2 \cdot xH_2O$), which was already observed in the IR spectra. (i) Assuming total water induced oxidation of the Si nanocrystallites from the nano-PS samples and (ii) taking into account that the oxidation of each Si atom is accompanied by the formation of two hydrogen molecules according to the following reaction: $Si + 2H_2O = SiO_2 + 2H_2$, an additional amount of the molecular hydrogen produced from the oxidation reaction B is estimated to reach to a value of 71 mmol/g. Thus, the maximum total amount of the molecular hydrogen issued because of the reactions A−B can be about 100 mmol per gram of the initial PS nanostructure. Such a theoretical value for the molecular hydrogen that can be obtained from the chemical treatment of the PS layers seems to be quite realistic, especially for the case of nano-PS powder consisting of the smallest (2−3 nm) amorphous Si nanocrystallites and, therefore, having the highest surface area and smaller nanocrystallite size.

In addition, we should add that the chemically induced production of the molecular hydrogen from the PS nanostructures appears to be much more efficient than that ensured by thermal annealing. However, the chemically stimulated hydrogen desorption is completely irreversible because of the complete transformation of the PS nanostructure into the hydrated dioxide.

IV. Energy Conversion Analysis

IV.1. Fuel Cell Generalities. Let us consider the case for which the hydrogen completely desorbed from the PS nanostructure is used to produce electricity through a fuel cell. The operation principle of a fuel cell is based on an oxidation−reduction reaction between hydrogen and oxygen which produces water, electricity, and heat:

$$H_2 \rightarrow 2H^+ + 2e^- \qquad \text{(anode)} \qquad (6)$$

$$\frac{1}{2}O_2 + 2H^+ + 2e^- \rightarrow H_2O \qquad \text{(cathode)} \qquad (7)$$

$$H_2 + \frac{1}{2}O_2 \rightarrow H_2O + \text{heat} \qquad \text{(total reaction)} \qquad (8)$$

Even if these three reaction products can be potentially used, only the electrical energy exploitation is further considered.

In zero-order approximation, all chemical energy issued from the reactions 8−10 and characterized by its enthalpy value, ΔH, is assumed to be transformed into electrical energy. All kinds of possible losses (reaction entropy, activation, ohmic, diffusion, etc.) are neglected. In such a case, the ideal fuel cell voltage, E_{ideal}, can be estimated according to the following relation:

$$E_{ideal} = -\frac{\Delta H}{2F} \qquad (9)$$

where F is Faraday's constant. At room temperature (25 °C) and atmospheric pressure (1 bar) $E_{ideal} = 1.23$ V for a low-temperature fuel cell. The case of the low-temperature fuel cells is considered for our further estimations. Moreover, the value of E_{ideal} is assumed to remain constant in time.

Electrical energy of a fuel cell, ξ (in J), can be expressed as follows:

$$\xi = \int p(t)\,dt = E_{ideal}\int_?^? i(t)\,dt = E_{ideal}Q_{total} \qquad (10)$$

where $p(t)$ is the electrical power, $i(t)$ is the current and Q_{total} (in C) is the total electrical charge liberated during the fuel cell functioning.

TABLE 1: Comparative Energetic Analysis of PS Nanostructures for Their Application as Hydrogen Reservoirs in Portable Devices

materials	atomic hydrogen content, (mmol g^{-1})	theoretical mass energy density, (W-h kg^{-1})	autonomy (h) of a device consuming 1 W and using 100 g of material storing hydrogen *(taking into account 50% efficiency of low-temperature fuel cell)*
meso-PS (90%, 10 nm)	13	429	21.4
nano-PS (90%, 5 nm)	34	1120	56.1
nano-PS powder (>95%, 2−3 nm)	66	2176	108.8
reversible metal hydrides[4]			
$MgH_2 \rightarrow Mg + H_2$	76	2505	125.2
$LaNi_5H_6 \rightarrow LaNi_5 + 3H_2$	14	461	23
hydride hydrolysis[4]			
$(NaBH_4 + 2H_2O) \rightarrow NaBO_2 + 4H_2$	108	3560	178
$(LiBH_4 + 4H_2O) \rightarrow LiOH + H_3BO_3 + 4H_2$	85	2802	140.1
hydride thermolysis[4]			
$NH_4BH_4 \rightarrow BN + 4H_2$	244	8043	402.1
$NH_3BH_3 \rightarrow BN + 3H_2$	195	6428	321.4
methanol reforming			
$(CH_3OH + H_2O) \rightarrow CO_2 + 3H_2$	120	3956	197.8
Li-ion batteries [(24)5] (for comparison)		150	15

According to eq 6, two moles of electrons can be extracted from each consumed mole of molecular hydrogen, Faradaic losses being neglected. Therefore, the total liberated electrical charge, Q_{total}, can be estimated as:

$$Q_{total} = N_H F \tag{11}$$

where N_H is the number of millimoles of atomic hydrogen stored per gram of PS.

Taking into account eqs 10 and 11, the mass energy density, ξ_M, (in W-h) obtained from one kilogram of PS can be estimated from the following relation:

$$\xi_M = \frac{E_{ideal} N_H F}{3600} \tag{12}$$

IV.2. Energetic Analysis of PS Nanostructures. Table 1 presents a comparative (with other hydrogen storage means) analysis of mass electrical energy that can be potentially extracted from the PS nanostructures through a fuel cell, taking into account atomic hydrogen concentrations measured experimentally as it is reported above. Only the maximal concentration values: 13, 34, and 66 mmol g^{-1} found in meso- and nano-PS structures with enhanced porosities (≥90%) are considered. Assuming quasi-identical levels for the fractal-like roughness of the specific surface for the PS nanostructures, the observed difference in hydrogen concentrations is explained by the similar difference in the mean dimension of the Si nanocrystallites constituting the PS samples. The higher the hydrogen concentration is, the higher the corresponding mass electrical energy is. The PS nanostructures consisting of Si nanocrystallites with a mean dimension of about 2 nm ensure a maximal mass electrical energy value of about 2200 W-h kg^{-1}, which is quite comparable with energy values ensured by other substances: hydrides and methanol. It is important to note that the autonomy of about 100 h could be ensured by the use of 100 g of PS nanostructures as hydrogen reservoirs for a portable device needing 1 W of electrical power.

V. Conclusions

Hydrogen content in porous silicon nanostructures has been quantitatively analyzed. The concentration of hydrogen chemically bound to the porous silicon specific surface is found to be strongly correlated to the dimension and shape of the Si nanocrystallites constituting the PS nanostructures. Maximal values of hydrogen concentration for both meso- and nano-PS samples are mainly due to the fractal-like shape of the nanocrystallite surface.[13,21] Chemical and thermal ways for hydrogen desorption have also been studied. Special efforts should be focused in the future on the elaboration of an approach ensuring reversible storage of hydrogen in PS nanostructures. We hope that the hydrogenated PS nanostructures can be used in the future as hydrogen source for Si-based fuel cells operating as energy suppliers in various portable devices.

Acknowledgment. FTIR measurements reported in this paper were performed using facilities of the CECOMO Measurement Center from Lyon Claude Bernard University. The authors are grateful to Prof. B. Champagnon and to all the staff of the center for their technical support.

References and Notes

(1) Mex, L.; Ponath, N.; Müller, J. *Fuel Cells Bull.* **2001**, *4*, 9.
(2) Meyers, J. P.; Maynard, H. L. *J. Power Sour.* **2002**, *109*, 76.
(3) Lee, S. J.; Chang-Chien, A.; Cha, S. W.; O'Hayre, R.; Park, Y. I.; Saito, Y.; Prinz, F. B. *J. Power Sources* **2002**, *112*, 410.
(4) *MRS Bull.* **2002**, *27*, 675.
(5) Herino, R. In *Properties of Porous Silicon*; Canham, L. T., Ed.; INSPEC, The IEE: London, 1997; p 89.
(6) Grosman, Ortega, C. In *Properties of Porous Silicon*; Canham, L. T., Ed.; INSPEC, The IEE: London, 1997; p 145.
(7) Buttard, D.; Dolino, G.; Faivre, C.; Halimaoui, A.; Comin, F.; Formoso, V.; Ortega, L. *J. Appl. Phys.* **1999**, *85*, 7105.
(8) Vázquez, E.; Tagüeña-Martínez, J.; Sansores, L. E.; Wang, C. *J. Appl. Phys.* **2002**, *91*, 3085.
(9) Kovalev, D.; Timoshenko, V. Yu.; Künzner, N.; Gross, E.; Koch, F. *Phys. Rev. Lett.* **2001**, *87*, 068301.
(10) Miculec, F. V.; Kirtland, J. D.; Sailor, M. J. *Adv. Mater.* **2002**, *14*, 38.
(11) Rivolo, P.; Geobaldo, F.; Rocchia, M.; Amato, G.; Rossi, A. M.; Garrone, E. *Phys. Status Solidi A* **2003**, *197*, 217.
(12) Martin, P.; Fernandez, J. F.; Sanchez, C. R. *Phys. Status Solidi A* **2000**, *182*, 255.
(13) Lysenko, V.; Vitiello, J.; Remaki, B.; Barbier, D.; Skryshevsky, V. *Appl. Surf. Sci.* **2004**, *230*, 425.
(14) Halimaoui, A. In *Properties of Porous Silicon*; Canham, L. T., Ed.; INSPEC, The IEE: London, 1997; p 12.

(15) Bruggeman, D. A. G. *Ann. Phys. (Leipzig)* **1935**, *24*, 636.

(16) See, for example: Campbell, H. Ph.; Fauchet, M. *Solid State Commun.* **1986**, *58*, 739.

(17) Chittur, K. K. *Biomaterials* **1998**, *19*, 357.

(18) Herino, R.; Bomchil, G.; Barla, K.; Bertrand, C.; Ginoux, J. L. *J. Electrochem. Soc.* **1987**, *134*, 1994.

(19) Timoshenko, V. Yu.; Osminkina, L. A.; Efimova, A. I.; Golovan, L. A.; Kashkarov, P. K.; Kovalev, D.; Künzner, N.; Gross, E.; Diener, J.; Koch, F. *Phys. Rev. B* **2003**, *67*, 113405.

(20) Wieder, H.; Cardona, M.; Guarnieri, C. R. *Phys. Status Solidi B* **1979**, *92*, 99.

(21) Nychyporuk, T.; Lysenko, V.; Barbier, D. *Phys. Rev. B* **2005**, *71*, 115402.

(22) Kitajima, M.; Ishioka, K.; Tateishi, S.; Nakanoya, K.; Fukata, N.; Murakami, K.; Fujimura, S.; Hishita, S.; Komatsu, M.; Haneda, H. *Mater. Sci. Eng., B* **1999**, *58*, 13.

(23) Gupta, P.; Dillon, A. C.; Bracker, A. S.; George, S. M. *Surf. Sci.* **1991**, *245*, 360.

(24) *Science of Synthesis: Houben-Weyl Methods of Molecular Transformations, Vol. 4: Compounds of Group 15 (As, Sb, Bi) and Silicon Compounds*, Fleming, I., Ed.; Georg Thieme Verlag: Stuttgart, Germany, 2001.

(25) Broussely, M.; Perton, F.; Labat, J.; Staniewicz, R. J.; Romero, A. *J. Power Sources* **1993**, *43*−*44*, 209.